Journal of Power Sources 467 (2020) 228353

Contents lists available at ScienceDirect

Journal of Power Sources

journal homepage: www.elsevier.com/locate/jpowsour

Enhanced capacitive behaviour of graphene based electrochemical double layer capacitors by etheric substitution on ionic liquids

Shirin Siyahjani [a], Saliha Oner [a,b], Halide Diker [a,c], Burak Gultekin [a], Canan Varlikli [a,c,*]

[a] Solar Energy Institute, Ege University, 35100, Bornova, Izmir, Turkey
[b] Chemistry Group, Middle East Technical University, Northern Cyprus Campus (METU NCC), Kalkanlı, Güzelyurt, Via Mersin 10, Turkey
[c] Department of Photonics, İzmir Institute of Technology, 35430, Urla, Izmir, Turkey

GRAPHICAL ABSTRACT

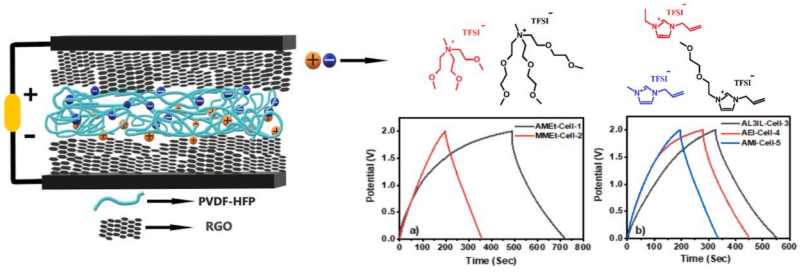

ARTICLE INFO

Keywords:
Gel polymer electrolyte
EDLC
Specific capacitance
Energy density
Viscosity

ABSTRACT

In this study, we report the effect of etheric substituents in imidazolium and ammonium based ionic liquids (IL) on the performance of electrochemical double layer capacitors (EDLC) consisted of gel polymer electrolyte (GPE) and reduced graphene oxide (RGO) electrode. GPEs contain poly (vinylidene fluoride-hexafluoropropylene) (PVDF-HFP) and the ILs. Ammonium and imidazolium based ionic liquids (ILs) differ by their length of etheric groups and etheric group contents, respectively. According to the cyclic voltammetry, galvanostatic charge-discharge and electrochemical impedance spectroscopy measurements, longer etheric group substituted {N-methyl-2-(2-methoxyethoxy)-N,N-bis[2- (2-methoxyethoxy)ethyl] ethan-1-aminium bis(trifluoromethanesulfonyl)imide (AMEt-TFSI) and ether substituted {3-allyl-1-[2-(2-methoxyethoxy)ethyl]-1H-imidazole-3-ium bis(trifluoromethanesulfonyl)imide (AL3IL-TFSI), tender specific capacitances of 250 Fg^{-1} and 238 Fg^{-1} and energy density values of 61.36 wh kg^{-1} and 61.56 wh kg^{-1}, respectively.

1. Introduction

In an electrochemical double layer capacitor (EDLC), capacitive behaviour is the result of charging at the interfaces between the electrolyte and electrodes which generally based on high surface area carbonaceous materials [1]. In order to obtain high energy density, most crucial parameters are the potential window related to the electrolyte and the capacitance related to both the electrode and electrolyte. Recently, ionic liquids (IL) have gained great interest in the energy storage applications due to their wide potential windows. Furthermore,

* Corresponding author. Department of Photonics, Izmir Institute of Technology, 35430, Urla, Izmir, Turkey.
E-mail addresses: s_siahjani@yahoo.com (S. Siyahjani), osaliha@metu.edu.tr (S. Oner), dikerhalide@gmail.com (H. Diker), burak.gultekin@ege.edu.tr (B. Gultekin), cananvarlikli@iyte.edu.tr, cananvarlikli@yahoo.co.uk (C. Varlikli).

https://doi.org/10.1016/j.jpowsour.2020.228353
Received 3 February 2020; Received in revised form 1 May 2020; Accepted 12 May 2020
Available online 22 May 2020

their variety in design, low melting points and high chemical stability under ambient conditions make them favorable for EDLC applications. However, only a few derivatives of ILs have been used in the electrochemical systems because of the physical properties of ILs such as the relative size of the ions and viscosity affecting the ionic conductivity which is a major element for electrochemical devices. Imidazolium, pyrrolidinium, piperidinium, pyrazolium and quaternary ammonium based ILs have been employed in EDLCs as electrolyte material. Since the low viscosity/high conductivity and ease of functionalization, 1, 3-dialkyl or 1,2,3-trialkylimidazolium ILs have been investigated in the literature extensively [2–4]. Pal et al. reported the ascending of specific capacitance values by the descending of cation size for imidazolium based ILs (1-butyl-2,3-dimethylimidazolium ($BDMI^+$), 1-butyl-3-methylimidazolium (BMI^+) and 1-ethyl-3-methylimidazolium (EMI^+) with tetrafluoroborate (BF_4^-) as the anion. It was proposed that ILs containing relatively smaller cation (EMI^+) size represent higher conductivity and higher accumulation on the electrode surface [5]. In another study, Senda and co-workers investigated the performance of imidazolium and pyrrolidinium cation based fluorohydrogenete ILs with activated carbon electrodes in EDLC applications. It was also determined that in the case of imidazolium based ILs, the maximum specific capacitance value was obtained with the smallest cation size IL (fluorohydrogenete 1,3-dimethylimidazolium ($DMIm^+$; 178 F g^{-1}). However, introduction of methoxy group in the cation changed this trend completely. In spite of the larger size of 1-methoxymethyl-1-methylpyrrolidinium ($MOMMPyr^+$) than that of 1-ethyl-1-methylpyrrolidinium ($EMPyr^+$), the maximum specific capacitance was achieved with the $MOMMPyr^+$ (152 F g^{-1}). It was claimed that the methoxy groups might change the charge distribution of the cation causing a relatively higher capacitance value [6]. Besides this, physical characterization results indicated that the methoxy group decreased the viscosity of the larger cation sized $MOMMPyr^+$ than that of $EMPyr^+$. Introducing electron-withdrawing (e.g. ester, cyano) [7,8] or electron-donating (e.g. ether) [9] groups on the cation can result in increment in the viscosity and melting point of the IL. These phenomena make it possible to design various types of low melting point ILs for EDLC applications. In addition to these, alkenyl functionalization has also attracted much attention to optimize the physical properties of ILs. In recent years, some highly conductive and low viscosity allylimidazolium based ILs with various anions have been reported [10]. Even though, the effect of the alkenyl groups on the physical parameters of the IL has not been clarified completely yet, it has been proposed that the π-π interactions between the double bonds on the side chains might cause few changes [11].

Although using ILs in an EDLC device as electrolyte is safer than using a liquid electrolyte, cell leakage is still an issue and in order to overcome this problem, immobilization of ILs in a polymer matrix is usually employed [12]. High viscosity of an IL is not a major disadvantage in GPEs, due to the decrement of ion-ion interactions in the polymer matrix which increases immobilization of the ions throughout GPEs [13]. Within the polar and non-polar polymers to be used in gel polymer electrolyte (GPE) systems, poly (vinylidene-co-hexafluoropropylene) PVDF-HFP copolymer gained attraction due to its high dielectric constant and good mechanical strength [5,14,15].

In this study, effects of etheric substituents on imidazolium and ammonium based cations on the performance of EDLC devices with reduced graphene oxide (RGO) electrodes have been investigated. For this purpose, three imidazolium based and two ammonium based ILs with TFSI anions were synthesized and utilized in PVDF-HFP as GPE components. EDLC devices were characterized by using cyclic voltammetry (CV), galvanostatic charge-discharge (GCD) and electrochemical impedance spectroscopic (EIS) techniques.

2. Experimental

2.1. Materials

All starting materials that were used for the synthesis of ionic liquids (ILs) were purchased from either Sigma-Aldrich or TCI (UK) and used without further purifications. Hydrazine monohydrate ($N_2H_4.H_2O$) and methanol were purchased from Merck. Carbon Black (CB, 99.9% S.A. 75 m^2/g) was obtained from Alfa Aesar. Poly (vinylidene fluoride-hexafluoropropylene) (PVDF-HFP) (average MW is about 400,000 g/mol) used as a binder in the electrode and host polymer of gel polymer electrolyte were also purchased from Sigma-Aldrich. Flexible graphite sheets with a thickness of 250 μm were used as a current collector and were supplied from Nickunj Eximp Enterprises.

2.2. Methods

Structural characterization of the ILs were done by using NMR spectroscopy, mass spectrometry and elemental analysis. ^1H NMR and ^{13}C NMR spectra were recorded on a Bruker Advance DPX 300 spectrometer (300 MHz). ESMS mass spectrometer measurements were carried out by using Waters LCT PREMIER Electrospray mass spectrometer (Micromass Technologies). Elemental analysis measurements were performed using a PerkinElmer Series II CHNS/O 2400 CHN Elemental Analyzer, which provided values within 0.3 wt% of error. Marvinsketch was used to determine ion sizes (Marvin V199.22, 2019, ChemAxon). Structural characterization of RGO and pure PVDF-HFP and GPEs films were performed by using Rigaku Ultima IV X-Ray Diffractometer (XRD), Thermo Scientific K-Alpha Surface Analysis XPS spectrometer and Horiba, XploRA Raman Microscope. A PerkinElmer Pyris 6 DSC instrument was used during the calorimetric characterization of polymer gel electrolytes. Fourier transform infrared (FT-IR) spectra were performed using a PerkinElmer Spectrum BX FTIR. The conductivity and electrochemical potential stability window (EPSW) of GPEs and the electrochemical behaviour of EDLC cells were analysed by using a CH Instrument CHI 660B.

2.3. Synthesis of ionic liquids

3-allyl-1-ethyl-1Himidazol- 3-ium bis(trifluoromethanesulfonyl) imide (AEI-TFSI) and 3-allyl-1-methyl-1H-imidazole-3-ium bis(trifluoromethanesulfonyl)imide (AMI-TFSI) ILs were synthesized according to literature [16,17]. The structures of synthesized ILs are given in Fig. 1. Details of the syntheses and characterization data of newly synthesized N-methyl-2-(2-methoxyethoxy)-N,N-bis[2- (2-methoxyethoxy)ethyl] ethan-1-aminium bis(trifluoromethanesulfonyl)imide (AMEt-TFSI), N-methyl-N-tris(2- methoxyethyl) ammonium bis(trifluoromethanesulfonyl)imide (MMEt-TFSI), 3-allyl-1-[2-(2-methoxyethoxy)ethyl]-1H-imidazole-3-ium bis(trifluoromethanesulfonyl)imide (AL3IL-TFSI), (AMI-TFSI) and (AEI-TFSI) are provided in the Supplementary Information (SI) document. Ammonium and imidazolium cations were combined with bis(trifluoromethanesulfonyl)imide ($TFSI^-$) anion for obtaining ILs which are molten at room temperature. Although significant decrements in viscosity values of ILs were observed by the increase in temperature from 20 °C to 80 °C, all synthesized ILs were viscous liquids at room temperature (Table S1). As a result, addition of ethoxy groups increased the fluidity for the ammonium based ILs and all synthesized ILs provided low viscosities in the range of 24–62 cP at 20 °C [18–20].

2.4. Synthesis of RGO

Graphene oxide (GO), which was synthesized by Hummers' method according to the procedure reported in our previous study [21], was used as the raw material for the reduction reaction. RGO sample was synthesized as described [22]; 32 mmol (1.55 ml) $N_2H_4.H_2O$ was added

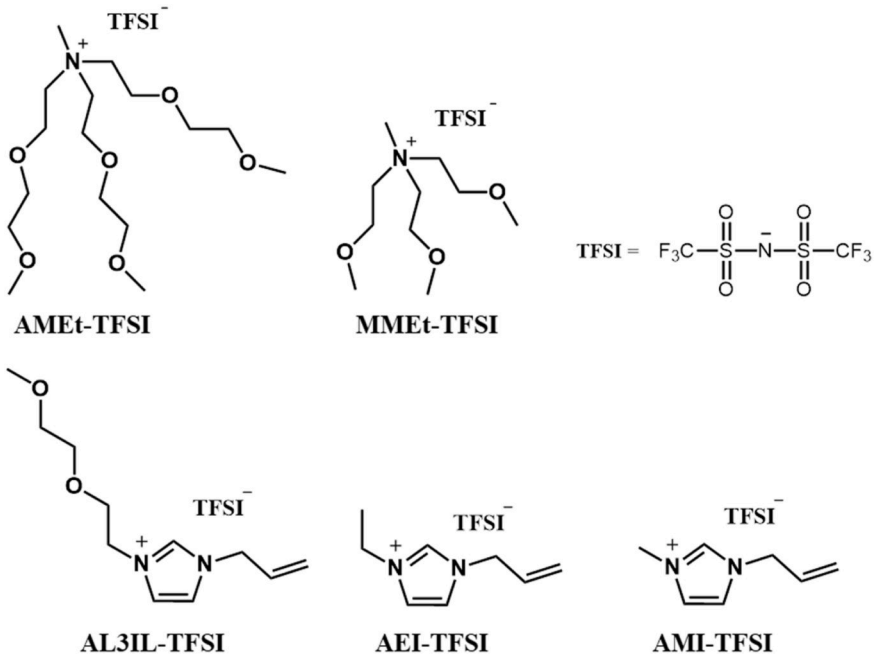

Fig. 1. Molecular structures of the ILs those are used in this study.

to 100 ml GO (1 mg/ml) aqueous dispersion and reduction reaction was carried out at 100 °C for 24 h. The reaction solution was filtered by washing with distilled water (500 ml) and methanol (500 ml), respectively. This filtered solid material was dried at 60 °C over-night.

2.5. Preparation of GPEs, electrode and fabrication of EDLC

GPE compositions of PVDF-HFP:IL with 1:0.5, 1:1, 1:1.5, 1:2, 1: 2.5, 1:3, 1:4, 1:5 and 1:6 wt ratios were prepared in acetone and magnetically stirred over-night at room temperature. Semi-transparent free-standing GPE films with thicknesses between 150 and 200 μm were obtained by transferring the solutions into a Petri dish and allowed to dry at room temperature. RGO powder, CB and PVDF-HFP in the weight ratio of 80:15:5 was grinded in mortar. Then, a small portion of acetone was added in the mixture to obtain homogeneous paste. The electrodes were prepared via coating the obtained paste on the graphite sheet current collector and keeping them in an oven over-night at 100 °C.

EDLC cells were fabricated by sandwiching the corresponding GPE between two symmetrical electrodes. The cells which contain PVDF-HFP:AMEt-TFSI, PVDF-HFP:MMEt-TFSI, PVDF-HFP:AL3IL-TFSI, PVDF-HFP:AEI-TFSI, PVDF-HFP:AMI-TFSI were named as Cell −1, −2, −3, −4 and 5, respectively. The area of the prepared EDLCs were approximately 1 cm^2 whereas, active material mass loading on each current collector was between 1 and 1.2 mg/cm^2.

3. Results and discussion

3.1. Characterization of RGO

C1s XPS spectrum of the RGO sample is given in Fig. S1a The peak of sp^2 C=C bonds (at ~ 284.5 eV) is more dominant than the peaks which are related to the oxygenated functional groups (*"C-O, ~285.7 eV"; "C = O, ~286.6 eV"; "O-C = O, 289.5 eV"*). The decrements in peak intensities of oxygenated functional groups on the RGO structure compared to those of GO reported in our previous study [21] points out to the success of reduction reaction (Fig. 2a). Additionally, C:O ratio increased approximately 4.1 folds after the reduction *i.e.; GO (C:O; 2.04), rGO (C:O; 8.4)*.

The success of reduction is further supported by XRD, TGA and Raman measurements. The characteristic peak of GO (~10°) shifted to a higher (2θ) value (~25°) for the RGO sample (Fig. 2b) and approached to the characteristic (2θ) peak of graphite (~26°) [23]. The sharp mass losses of GO at 230 °C was not observed for the RGO as the oxygenated functional groups were reduced and GO was consumed at 650 °C whereas, ~61% of the mass of RGO was preserved at this temperature (Fig. S1b). Additionally, compared to GO ("*G:* 1588 cm^{-1};

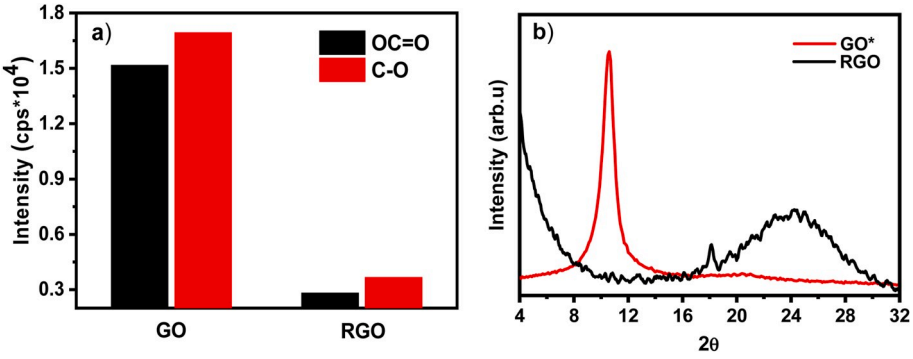

Fig. 2. (a) the peak intensity graphs of oxygenated functional groups on the GO and RGO structures that are extracted from O1s binding energy spectrum. (b) XRD patterns of GO and RGO *(Characterization results of GO are from our previous study* [21]*)*.

"ID/IG:0.98"), the slight redshift at the G band RAMAN peak (1585,6 cm^{-1}), and increment in I_D/I_G (1.06) ratio were considered as other pieces of evidence of the effective reduction of the RGO (Fig. S1c) [24,25].

The Brunauer-Emmett-Teller (BET) analysis was used to determine the porosity character of RGO. N_2 adsorption–desorption isotherms exhibited type-IV characteristics with the given hysteresis in the 0.4–1.0 of relative pressure range, indicated the presence of mesoporosity (Fig. S2a). Cumulative pore volume and differential pore volume curves for N_2 absorption demonstrated that the size of well-defined mesopores was less than 8 nm and the average diameter of pores was 4.7 nm (Fig. S2b). Additionally, the specific surface area of RGO was obtained as 413.44 ± 2.72 m^2/g which is quite sufficient for EDLC applications according to literature studies [26].

3.2. Physicochemical characterization of GPEs

Ionic conductivity (δ) of each GPE were calculated with the data obtained through electrochemical impedance spectroscopy (EIS) in the frequency range of 10 mHz–100 KHz and via using the below equation [27].

$$\delta = \frac{l}{R_b \ S}$$

where l is the distance between the two electrodes (thickness of GPE), S is cross sectional area of electrode and R_b is bulk resistance [28]. The conductivity of composite electrolyte increased gradually by the increasing amount of IL until the PVDF HFP:IL weight ratio of 1:5 (Fig. 3) is reached. Calculated maximum ionic conductivity values are summarized in Table 1. Despite relatively higher cationic size (CS) and viscosity (η) of ether functionalized ammonium based ILs, δ values of the GPEs owing these ILs were higher than those of the GPEs with imidazolium based ILs. Two reasons can be proposed for this situation both of which serve lowered physical interaction between the polymer matrix and the IL; (*i*) the hydrophobic character of PVDF-HFP, may have allowed mobilization of cationic etheric groups, which have relatively higher hydrophilic character and (*ii*) the 3D structure of ammonium based cations prevented stacking probability which might have occurred in the π-system of imidazolium cations [13]. Similar etheric group effect was also observed between the ether functionalized [AL3IL (CS: 0.71 nm, η: 41 mPa)] and the alkyl functionalized [AEI (CS: 0.44 nm, η: 20 mPa) and AMI (CS: 0.41 nm, η: 24 mPa)] imidazolium based ILs. Even the cationic size and viscosity of AL3I-TFSI are very high compared to those of AEI-TFSI and AMI-TFSI, the conductivities of GPEs owing these imidazolium based ILs were in the same range.

In addition to the ionic conductivity, liner sweep voltammetry measurements were carried out for the determination of the electrochemical stability window (ESW) of the GPEs (Fig. 4). Obtained results indicate that GPEs owing the ammonium based ILs [AMEt-GPE-1 (−2.9–2.6 V), MMEt-GPE-2 (−2.9–2.5 V)] have higher ESWs than those of GPEs owing imidazolium based ILs [AL3IL-GPE-3 (−2.9–2.0 V), AEI-GPE-4 (−2.8–2.0 V), AMI-GPE-5 (−2.6–2.0 V)] (Table 1). In an ionic liquid based GPE, oxidation and reduction processes are related to the anion and the cation of the IL, respectively and quaternary ammonium salts are known to exhibit higher ESWs than those of imidazolium salts with their relatively lower LUMO energy levels [29]. All ILs used in GPEs have the same anion, and as expected $TFSI^-$ exhibited oxidation potentials higher than 2.0 V [30,31]. However, the oxidation potentials recorded with imidazolium based GPEs were lower than those of ammonium based ones. This is attributed to the relatively high HOMO energy level of imidazolium and its potential to effect on both the oxidation and the reduction processes [18,32]. The higher reduction potential measured for GPE owing AL3IL-TFSI than those of AMI-TFSI and AEI-TFSI are attributed to the electron donating behaviour of etheric side chain on AL3IL cation.

Table 1
Cationic size (CS) and viscosity (η) of ILs together with the maximum ionic conductivity (δ) and electrochemical stability windows (ESW) of GPEs.

Electrolyte	CS of IL (nm)[a]	η of IL mPa (@25 °C)	Maximum δ[b] (S/cm)	ESW (V)
AMEt-GPE-1	0.95	50	1.30×10^{-4}	−2.9 to 2.5
MMEt-GPE-2	0.64	44	1.45×10^{-4}	−2.9 to 2.5
AL3IL-GPE-3	0.71	41	3.90×10^{-5}	−2.9 to 2.1
AEI-GPE-4	0.44	28	5.20×10^{-5}	−2.8 to 2.0
AMI-GPE-5	0.43	24	2.90×10^{-5}	−2.6 to 2.0

[a] Calculated by Marvinsketch (Marvin V199.22,2019, ChemAxon).
[b] For PVDF-HFP:IL weight ratio of 1:5.

The physical behaviour of interactions between the polymer matrix and ILs and the proposed impact on conductivity were supported by XRD and DSC measurements. The four characteristic semi-crystalline peaks of host polymer PVDF-HFP at 2θ ≈ 18°, 19.8°, 26.5° and 38.8°, which correspond to (100), (110), (022) and (211) crystalline planes, respectively [15,33] were present in the XRD spectrum (Fig. 5). Although no diffraction angle shifts were detected, diffraction peak at 26.5° disappeared completely in all patterns of GPEs and the intensity descending

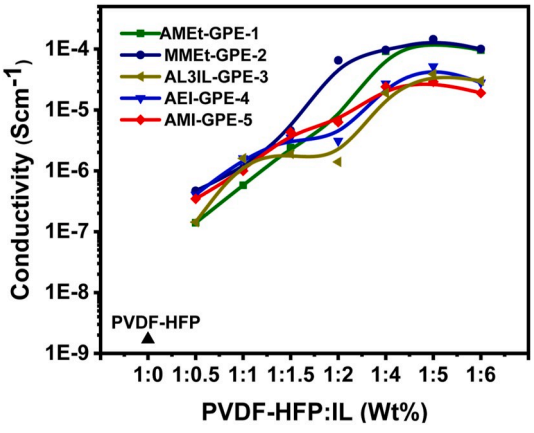

Fig. 3. Ionic conductivity of GPE with various PVDF-HFP:IL ratios.

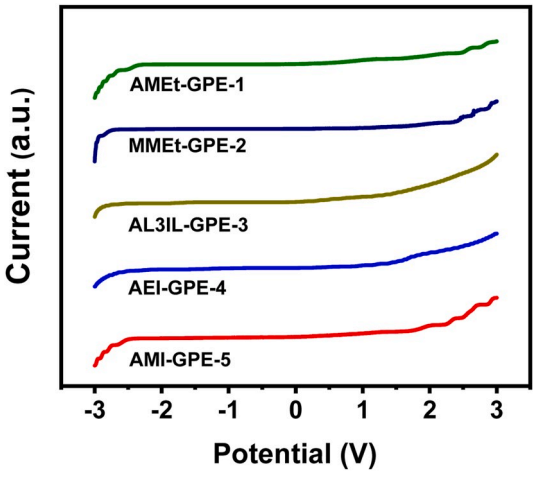

Fig. 4. Liner sweep voltammograms of GPEs in weight ratio of 1:5 (PVDF HFP:IL) [Bare PVDF-HFP presents neither oxidation nor reduction in the range of -6 V to +6 V (Fig. S3) confirming the electrochemical stability of the polymer matrix in the determined working potential windows of all GPEs.].

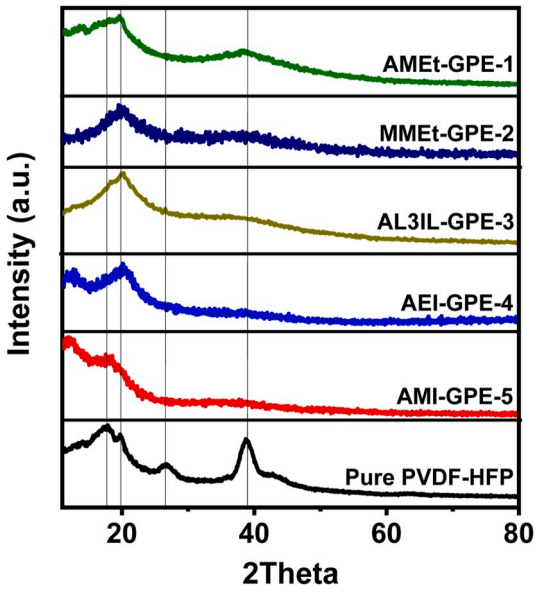

Fig. 5. XRD patterns of Pure PVDF-HFP and GPEs.

and full width of half maximum (FWHM) ascending at 18° and 38.8° in patterns of GPEs were determined. These results indicated that addition of ILs into the polymer matrix decreased the crystallinity of polymer in the GPEs. However, for the GPEs owing ammonium and etheric side chain containing imidazolium based ILs, the intensity decrements and FWHM increments at 18° and 38.8°, respectively, were lower than those of the others. This situation suggests that, to some extent, the semi-crystalline structure of PVDF-HFP was prevented in these GPEs as a result of hydrophobicity and hydrophilicity mismatch between the polymer and ILs.

DSC analyses were carried out to determine the fraction of amorphous phase in the GPEs (Fig. S4a). DSC measurement of pure PVDF-HFP and GPE films were recorded at a heating rate of 10 °C min^{-1} under nitrogen environment. The weights of the GPE samples were maintained in the range of 5–6 mg. The melting point of pure host polymer PVDF-HFP film was observed at around 140 °C as a sharp endothermic peak. The melting points of the GPEs were shifted to lower temperatures with more asymmetrical and wider shapes due to the descending of the crystallinity by the insertion of ILs into the host polymer matrix [27]. The degree of crystalline fraction (X_C) for each GPE were calculated by using following equation [34];

$$X_C = \frac{\Delta H_m}{\Delta H_m^\circ} \times 100\%$$

where $\Delta H^0_m \sim 104.7$ J g^{-1} is the melting enthalpy for 100% crystalline PVDF-HFP polymer matrix and ΔH_m is melting enthalpy of ionic liquid doped gel electrolytes, which was obtained by calculating the area under the melting point peaks. Obtained T_m and calculated, ΔH_m and X_c values are summarized in Table 2. Obtained results illustrate that ammonium based GPEs have slightly lower melting enthalpy. It may be suggested that 3D structured ammonium based cations increase the distance between the polymer chains and decrease the degree of crystallization more than the imidazolium based cations. Further support on the decreasing crystallinity was obtained from FTIR measurements (Fig. S4 (b), (c)). These findings support the reasons proposed above on the lower degree of physical interaction and increasing conductivity as a result of easier ion transport in the polymer matrix [5].

Table 2
T_m, ΔH_m and X_c values of pure polymer and GPEs.

Electrolyte	T_m (°C)	ΔH_m (J g^{-1})	X_c (%)
Pure PVDF-HFP	140.97	41.60	39.7
AMEt-GPE-1	89.28	4.20	4.0
MMEt-GPE-2	91.11	3.90	3.7
AL3IL-GPE-3	94.94	5.80	5.5
AEI-GPE-4	90.95	5.89	5.6
AMI-GPE-5	91.44	6.59	6.2

3.3. Electrochemical performance of supercapacitor cells

3.3.1. Electrochemical impedance spectroscopy (EIS)

EIS was used to understand the electrical behaviour of the bulk materials in the devices and their interfacial resistance. As demonstrated in Fig. 6, Nyquist plots for the frequency window of 10 mHz–100 kHz, exhibit a straight line at the low frequency region and a semicircle at the high frequency region. As discussed above in section 3.2, the existence of etheric bonds in both ammonium and imidazolium based ionic liquids provided a significant positive contribution to the conductivity of gel electrolytes and its consecutive effects on EIS parameters are noticeable. In ammonium based cells the bulk resistance of MMEt-cell-2 (7.0 Ω cm^2) was lower than that of AMEt-cell-1(10.0 Ω cm^2) which can be attributed to bigger CS of AMEt than that of MMEt (Table 2). However, the trend of obtained bulk resistance in imidazolium based cells is AL3IL-cell-3 (8.0 Ω cm^2) > AEI-cell-4 (13.0 Ω cm^2) > AMI-cell-5 (22.0 Ω cm^2). Unlike the ammonium based cells, the bulk resistance of AL3IL-Cell-3 with the largest CS had the lower R_b than the purely allyl counterparts. The same trends were observed also in R_{ct} value of both ammonium and imidazolium based cells. It can be proposed that relatively planar structure of purely allyl functionalized imidazolium cations (AEI and AMI) might form aggregates via π-π stacking [10]. These aggregates cannot travel easily to the electrode surface under AC signal. Besides this, steric effect of ether chain on the imidazolium (AL3IL) decreases the aggregation ratio of the cations [35]. The overall capacitance of EDLC cell is calculated from

$$C = -\frac{1}{2\pi f.Z''}$$

where Z″ is the imaginary part of impedance and *f* is the frequency of the applied AC signal in Hz [36]. The specific capacitance values of ammonium based cells is in the order of AMEt-Cell-1 (208 F g^{-1}) > MMEt-Cell-2 (154 F g^{-1}) and for the case of imidazolium based electrolytes, the trend is AL3IL-Cell-3 (170 F g^{-1}) > AEI-Cell-4 (164 F g^{-1}) > AMI-Cell-5 (122 F g^{-1}) (Table 3). It is observed that the value of the specific capacitance of the EDLCs obtained from EIS increases by increasing the length of the ether chain in ammonium based cell. However, in the imidazolium based cells, the highest specific capacitance value was achieved by the cell using AL3IL-GPE-3 in comparison to those of using purely allyl counterparts. It can be proposed that increased flexibility by etheric bond on the cations might ease the movement of them in the pores of electrode material, resulting a performance improvement. In addition to this, a weak negative region occurs on the etheric chains of the cations. This region allows cations to approach each other easily and place in the pore denser [9]. Therefore, by introducing etheric side groups to the cations, even though the IL become more viscous and less conductive, greater amount of charge can be stored in the device via more suitable physical properties.

3.3.2. Cyclic voltammetry

Charge storage properties of the electrode-electrolyte interfaces can be determined by cyclic voltammetry (CV) studies of EDLCs. Fig. S5 exhibits the cyclic voltammograms of AMEt-Cell-1, MMEt-Cell-2, AL3IL-Cell-3, AEI-Cell-4 and AMI-Cell-5 at different scan rates in the voltage range of −1.0 V to +1.0 V at room temperature. It is observed that all cells present a reversible capacitive characteristic of a double layer at the electrode-electrolyte interface [15]. Fig. 7a and b shows the comparison of the CV of the supercapacitor cells at 50 mV s^{-1} scan rate in the

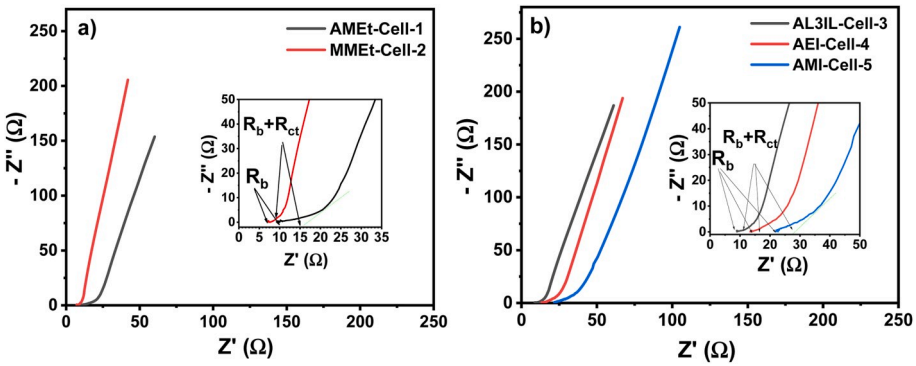

Fig. 6. Impedance plots for (a) ammonium based cells (b) imidazolium based cells. The inset shows the magnified view of the complex impedance plots in the high frequency region.

Table 3
Bulk resistance (R_b), charge transfer resistance (R_{ct}), specific capacitance calculated from CV at range of −2 V to +2 V and specific capacitance calculated from EIS.

Device	R_b (Ωcm^2)	R_{ct} (Ω cm^2)	Capacitance (F g^{-1}) CV	Capacitance (F g^{-1}) EIS
AMEt-Cell-1	10	5.0	192	208
MMEt-Cell-2	7.0	1.0	170	154
AL3IL-Cell-3	8.0	4.0	190	170
AEI-Cell-4	13	5.0	160	164
AMI-Cell-5	22	6.0	120	122

voltage range of −2.0 V to +2.0 V. The capacitance values from CV were evaluated using the below equation

$$C = \frac{i}{ms}$$

where i is the average current, m is the average mass of electrode materials (including binder and additive) and s is the scan rate ($\Delta V/\Delta t$). The variation of specific capacitance values calculated from CV curves by different scan rates for both ammonium and imidazolium based cells are presented in Fig. 7c. While the scan rate increases, specific capacitance decreases significantly for all cells. The reason for that is, at lower scan rates, ions contributing to the capacitance can arrive to the pores and accumulate on the surface of the electrodes easily. However, those charge carriers have not enough time to penetrate and assemble into the pores regularly at higher scan rates [37]. It was also observed that the value of specific capacitance at scan rate of 50 mV s^{-1} is in the order of AMEt-Cell-1 (192 F g^{-1}) > MMEt-Cell-2 (170 F g^{-1}) for ammonium

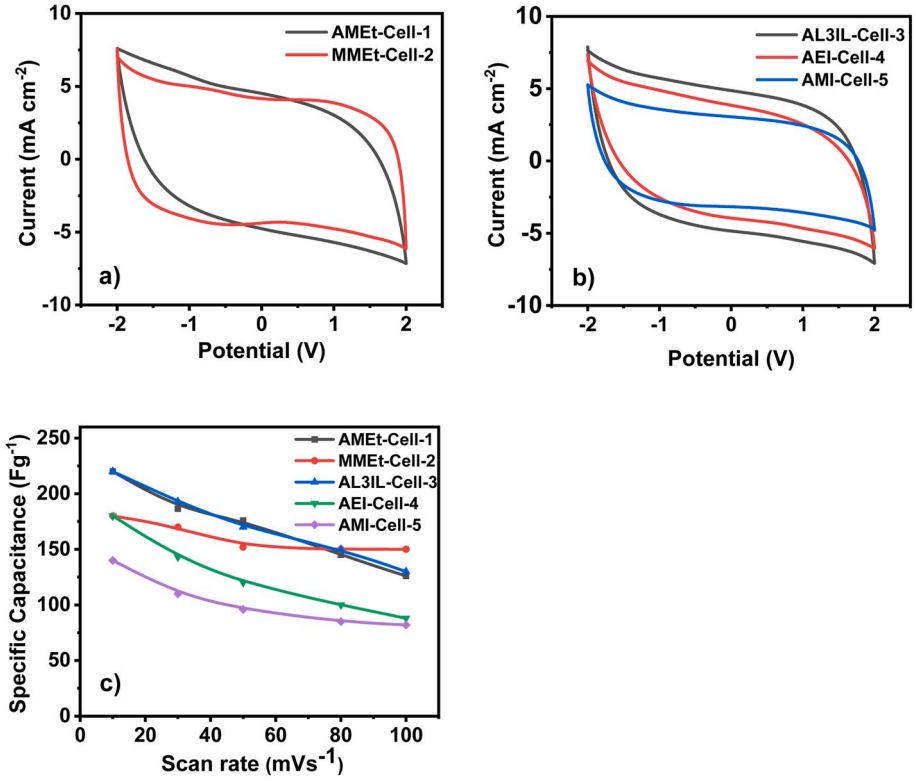

Fig. 7. Comparison of Cyclic Voltammetry for (a) ammonium based cells, (b) imidazolium based cells at a scan rate of 50 mV s^{-1} (c) Variation of specific capacitance obtained from CV with scan rate for different cells (data extracted from Fig. S5).

based cells (Fig. 7a) and AL3IL-Cell-3(190 F g^{-1}) > AEI-Cell-4(160 F g^{-1}) > AMI-Cell-5(120 F g^{-1}) for imidazolium based cells (Fig. 7b) which is in good agreement with the EIS data. The AMEt-Cell-1 (with larger CS and higher η) showed higher specific capacitance than the MMEt-Cell-2. Above mentioned formation of weak negative region effect is more dominant in AMEt-Cell-1 than in MMEt-Cell-2 due to the longer ether chains. Furthermore, CV measurements for different voltage ranges at a fixed scan rate of 50 mV s^{-1} were carried out to determine the electrochemical potential window of gel electrolytes. It can be observed that voltammograms remain in almost rectangular-like shape with gradual increase of voltage range for all devices (Fig. S6). These results are consistent with the wide range ESWs of GPEs shown earlier in Fig. 5.

3.3.3. Galvanostatic charge-discharge (GCD) characteristics

The GCD technique was used to determine the gravimetric capacitance and equivalent series resistance (ESR) of prepared EDLC cells. A comparative representation of charge-discharge responses of ammonium and imidazolium based cells can be seen in Fig. 8a and b at a constant current rate of 1.0 mA cm^{-2}. All charge-discharge curves have a barely linear characteristics indicating that all of the fabricated devices represent a general double-layer capacitive behaviour [38]. In addition, overall internal resistance for each electrochemical cell was calculated from the sudden voltage drop in the corresponded charge-discharge curve. It can be noted that the resistance values obtained by EIS are related to the material properties such as electrolyte and electrolyte-electrode interface etc., while the ESR is the overall cell resistance, when cell is under operation. In other words, ESR is a practical working resistance of the cell [39]. Therefore, evaluated ESR from GCD analyses is slightly higher than those of obtained resistance values from EIS measurement. The specific capacitance values calculated at 1.0 mA cm^{-2} discharge current for each cell (Table 4) were found to be comparable with the values obtained from the impedance and cyclic voltammetry studies. Besides these, all devices were charged and discharged at various current rates from 0 to 2.0 V at room temperature (Fig. S7). In order to understand the ion transport dynamics in the devices, GCD curves were recorded under different discharge currents (1.0 $mAcm^{-2}$, 1.5 $mAcm^{-2}$, 2.0 $mAcm^{-2}$, 2.5 $mAcm^{-2}$, 3.0 $mAcm^{-2}$, 3.5 $mAcm^{-2}$, 4.0 $mAcm^{-2}$) and specific capacitance as a function of discharge current plots for each cell were obtained (Fig. 8c). As it can be clearly seen that even a descending occurs under high discharge currents, the cells keep their capacitive behaviour. However, highest capacitance loss rate was monitored during GCD analysis of AMEt-Cell-1 containing the largest cation.

Table 4
Values of ESR, gravimetric specific capacitance, energy density and power density at a constant current 1.0 mA cm^{-2} obtained from charge-discharge characteristics for different cells.

Device	ESR (Ωcm^2)	Capacitance GCD (F/g)	Energy density (wh kg^{-1})	Power density (kw kg^{-1})
AMEt-Cell-1	50	250	61.36	0.940
MMEt-Cell-2	15	160	43.21	0.972
AL3IL-Cell-3	27.5	238	61.56	0.962
AEI-Cell-4	31.5	176	40.86	0.961
AMI-Cell-5	26.0	146	37.37	0.960

Energy and power densities were calculated from the GCD measurements. The semi solid-state supercapacitors containing AMEt-GPE-1 and AL3IL-GPE-3 electrolyte achieved relatively higher energy density due to their high capacitance and electrochemical stability window. The energy and power density values of all cells at various current densities were presented as Ragone Plot (Fig. 8d) indicating the relation between them. The energy density of cells linearly decreases by the increasing of power density for all cells, which means that less energy is released at higher power outputs and higher discharge currents [15]. However, this energy loss is more significant for AMEt-Cell-1 and AL3IL-Cell-3 that

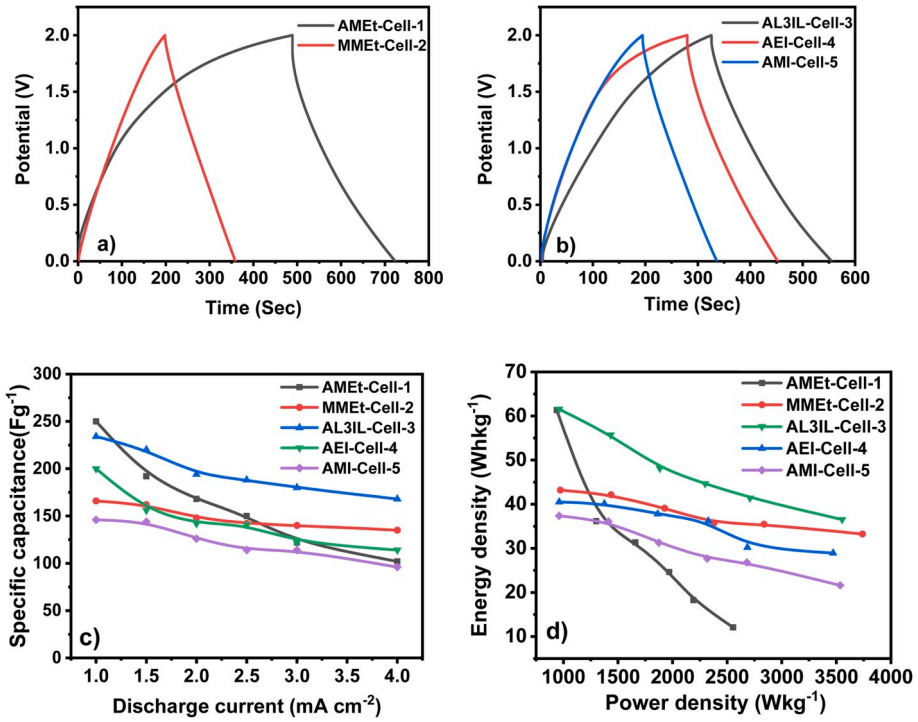

Fig. 8. Comparison of galvanostatic charge-discharge of (a) ammonium based cells (b) imidazolium based at constant current of 1.0 mA cm^{-2}. (c) Variation of specific capacitances obtained from galvanostatic charge-discharge (data extracted from Fig. S7) with different discharge currents for all EDL capacitor cells. (d) Ragone plots (gravimetric specific energy versus specific power) for all EDL capacitor cells.

have larger cation sizes.

4. Conclusion

In summary, imidazolium and ammonium based GPEs were prepared and EDLC devices were fabricated. Effects of the presence and the length of etheric groups in the IL on supercapacitor performance were investigated. The conductivity of GPEs based on AMI-TFSI (2.90×10^{-5} S cm^{-1}), AEI-TFSI (5.20×10^{-5} S cm^{-1}), AL3IL-TFSI (3.90×10^{-5} S cm^{-1}), MMEt-TFSI (1.45×10^{-4} S cm^{-1}) and AMEt-TFSI (1.30×10^{-4} S cm^{-1}) were determined. Obtained results demonstrated that the presence of ether groups on the ions might change the inverse proportion between the ion size/viscosity and conductivity of an ionic liquid in the GPE application due to the interaction between the ions and polymer chains. In addition to this, the capacitance values of fabricated EDLC by using GPEs were calculated by CV, EIS and GCD techniques. AMEt-TFSI containing longer ether chains than that of MMEt-TFSI represented the highest capacitance performance, while ether group functionalized imidazolium based AL3IL-TFSI represented the best performance among imidazolium based ILs. Results indicated that the presence of etheric groups in imidazolium based ILs and the longer etheric groups in ammonium based ILs, could increase the capacitance due to the denser packaging of ions on the electrode surface. Besides this, highest energy density values were also obtained with the supercapacitors based on AMEt-TFSI (61.36 wh kg^{-1}) and AL3IL-TFSI (61.56 wh kg^{-1}) which have larger working voltage windows.

Declaration of competing interest

The authors declare that they have no known competing financial interests or personal relationships that could have appeared to influence the work reported in this paper.

CRediT authorship contribution statement

Shirin Siyahjani: Methodology, Validation, Formal analysis, Investigation, Writing - original draft. **Saliha Oner:** Methodology, Validation, Formal analysis, Investigation, Writing - original draft. **Halide Diker:** Methodology, Validation, Formal analysis, Investigation, Writing - original draft. **Burak Gultekin:** Formal analysis, Writing - original draft. **Canan Varlikli:** Conceptualization, Writing - review & editing, Supervision, Project administration.

Acknowledgements

S.S. and C.V. would like to thank Prof. Dr. Pramod Singh Kumar and Prof. Dr. Yogesh Kumar for their theorical contribution during the evaluation of EDLC results. S.O and C.V. are thankful to Dr. H. Q. Nimal Gunaratne for the productive discussions and contributions related with the synthesis and characterization of the ILs. We would also like to acknowledge the Ministry of Development of Turkey for the project supports for some of the consumables (project #: 16 DPT002) and infrastructure (project #: 11DPT003). H.D. and C.V. thank to the project support of Scientific and Technological Research Council of Turkey (TUBITAK) (Project #: 114M508) for the synthesis and characterizations of graphene derivatives and for the fellowship support for HD. We would also like to thank the Izmir Institute of Technology, The Centre for Materials Research for BET analysis.

Appendix A. Supplementary data

Supplementary data to this article can be found online at https://doi.org/10.1016/j.jpowsour.2020.228353.

References

[1] L.L. Zhang, R. Zhou, X.S. Zhao, Graphene-based materials as supercapacitor electrodes, J. Mater. Chem. 20 (2010) 5983–5992, https://doi.org/10.1039/c000417k.
[2] Y.-Z. Su, Y.-C. Fu, J.-W. Yan, Z.-B. Chen, B.-W. Mao, Double layer of Au(100)/ionic liquid interface and its stability in imidazolium-based ionic liquids, Angew. Chem. 121 (2009) 5250–5253, https://doi.org/10.1002/ange.200900300.
[3] G.P. Pandey, S.A. Hashmi, Ionic liquid 1-ethyl-3-methylimidazolium tetracyanoborate-based gel polymer electrolyte for electrochemical capacitors, J. Mater. Chem. 1 (2013) 3372–3378, https://doi.org/10.1039/c2ta01347a.
[4] S. Zhang, N. Sun, X. He, X. Lu, X. Zhang, Physical properties of ionic liquids: database and evaluation, J. Phys. Chem. Ref. Data 35 (2006) 1475–1517, https://doi.org/10.1063/1.2204959.
[5] P. Pal, A. Ghosh, Solid-state gel polymer electrolytes based on ionic liquids containing imidazolium cations and tetrafluoroborate anions for electrochemical double layer capacitors: influence of cations size and viscosity of ionic liquids, J. Power Sources 406 (2018) 128–140, https://doi.org/10.1016/j.jpowsour.2018.10.051.
[6] A. Senda, K. Matsumoto, T. Nohira, R. Hagiwara, Effects of the cationic structures of fluorohydrogenate ionic liquid electrolytes on the electric double layer capacitance, J. Power Sources 195 (2010) 4414–4417, https://doi.org/10.1016/j.jpowsour.2010.01.055.
[7] F. Mazille, Z. Fei, D. Kuang, D. Zhao, S.M. Zakeeruddin, M. Grätzel, P.J. Dyson, Influence of ionic liquids bearing functional groups in dye-sensitized solar cells, Inorg. Chem. 45 (2006) 1585–1590, https://doi.org/10.1021/ic051751a.
[8] J.S. Lee, N.D. Quan, J.M. Hwang, J.Y. Bae, H. Kim, B.W. Cho, H.S. Kim, H. Lee, Ionic liquids containing an ester group as potential electrolytes, Electrochem. Commun. 8 (2006) 460–464, https://doi.org/10.1016/j.elecom.2006.01.009.
[9] A.J.R. Rennie, N. Sanchez-Ramirez, R.M. Torresi, P.J. Hall, Ether-bond-containing ionic liquids as supercapacitor electrolytes, J. Phys. Chem. Lett. 4 (2013) 2970–2974, https://doi.org/10.1021/jz4016553.
[10] A. Orita, K. Kamijima, M. Yoshida, Allyl-functionalized ionic liquids as electrolytes for electric double-layer capacitors, J. Power Sources 195 (2010) 7471–7479, https://doi.org/10.1016/j.jpowsour.2010.05.066.
[11] T. Mizumo, E. Marwanta, N. Matsumi, H. Ohno, Allylimidazolium halides as novel room temperature ionic liquids, Chem. Lett. 33 (2004) 1360–1361, https://doi.org/10.1246/cl.2004.1360.
[12] Y.K. Ahn, B. Kim, J. Ko, D.J. You, Z. Yin, H. Kim, D. Shin, S. Cho, J. Yoo, Y.S. Kim, All solid state flexible supercapacitors operating at 4 v with a cross-linked polymer-ionic liquid electrolyte, J. Mater. Chem. 4 (2016) 4386–4391, https://doi.org/10.1039/c6ta00643d.
[13] Y.S. Ye, J. Rick, B.J. Hwang, Ionic liquid polymer electrolytes, J. Mater. Chem. 1 (2013) 2719–2743, https://doi.org/10.1039/c2ta00126h.
[14] X. Yang, F. Zhang, L. Zhang, T. Zhang, Y. Huang, Y. Chen, A high-performance graphene oxide-doped ion gel as gel polymer electrolyte for all-solid-state supercapacitor applications, Adv. Funct. Mater. 23 (2013) 3353–3360, https://doi.org/10.1002/adfm.201203556.
[15] P. Pal, A. Ghosh, Highly efficient gel polymer electrolytes for all solid-state electrochemical charge storage devices, Electrochim. Acta 278 (2018) 137–148, https://doi.org/10.1016/j.electacta.2018.05.025.
[16] Z. Fei, D. Kuang, D. Zhao, C. Klein, W.H. Ang, S.M. Zakeeruddin, M. Grätzel, P. J. Dyson, A supercooled imidazolium iodide ionic liquid as a low-viscosity electrolyte for dye-sensitized solar cells, Inorg. Chem. 45 (2006) 10407–10409, https://doi.org/10.1021/ic061232n.
[17] P. Bonhôte, A.-P. Dias, N. Papageorgiou, K. Kalyanasundaram, M. Grätzel, Hydrophobic, highly conductive ambient-temperature molten salts †, Inorg. Chem. 35 (1996) 1168–1178, https://doi.org/10.1021/ic951325x.
[18] Z.-B. Zhou, H. Matsumoto, K. Tatsumi, Cyclic quaternary ammonium ionic liquids with perfluoroalkyltrifluoroborates: synthesis, characterization, and properties, Chem. Eur J. 12 (2006) 2196–2212, https://doi.org/10.1002/chem.200500930.
[19] L.C. Branco, J.N. Rosa, J.J. Moura Ramos, C.A.M. Afonso, Preparation and characterization of new room temperature ionic liquids, Chem. Eur J. 8 (2002) 3671, https://doi.org/10.1002/1521-3765(20020816)8:16<3671::AID-CHEM3671>3.0.CO;2-9.
[20] G.D. Smith, O. Borodin, L. Li, H. Kim, Q. Liu, J.E. Bara, D.L. Gin, R. Nobel, A comparison of ether- and alkyl-derivatized imidazolium-based room-temperature ionic liquids: a molecular dynamics simulation study, Phys. Chem. Chem. Phys. 10 (2008) 6301–6312, https://doi.org/10.1039/b808303g.
[21] H. Diker, G.B. Durmaz, H. Bozkurt, F. Yeşil, C. Varlikli, Controlling the distribution of oxygen functionalities on GO and utilization of PEDOT:PSS-GO composite as hole injection layer of a solution processed blue OLED, Curr. Appl. Phys. 17 (2017) 565–572, https://doi.org/10.1016/j.cap.2017.02.002.
[22] S. Stankovich, D.A. Dikin, R.D. Piner, K.A. Kohlhaas, A. Kleinhammes, Y. Jia, Y. Wu, S.T. Nguyen, R.S. Ruoff, Synthesis of graphene-based nanosheets via chemical reduction of exfoliated graphite oxide. https://doi.org/10.1016/j.carbon.2007.02.034, 2007.
[23] S. Abdolhosseinzadeh, H. Asgharzadeh, H. Seop Kim, Fast and fully-scalable synthesis of reduced graphene oxide, Sci. Rep. 5 (2015) 10160, https://doi.org/10.1038/srep10160.
[24] V.H.V.H. Pham, T.V.T.V. Cuong, S.H.S.H. Hur, E. Oh, E.J.E.J. Kim, E.W.E.W. Shin, J.S.J.S. Chung, Chemical functionalization of graphene sheets by solvothermal reduction of a graphene oxide suspension in N-methyl-2-pyrrolidone, J. Mater. Chem. 21 (2011) 3371–3377, https://doi.org/10.1039/c0jm02790a.
[25] P. Solís-Fernández, R. Rozada, J.I. Paredes, S. Villar-Rodil, M.J. Fernández-Merino, L. Guardia, A. Martínez-Alonso, J.M.D. Tascón, Chemical and microscopic analysis

of graphene prepared by different reduction degrees of graphene oxide, J. Alloys Compd. 536 (2012) S532–S537, https://doi.org/10.1016/j.jallcom.2012.01.102.
[26] M. Wang, L.D. Duong, N.T. Mai, S. Kim, Y. Kim, H. Seo, Y.C. Kim, W. Jang, Y. Lee, J. Suhr, J. Do Nam, All-solid-state reduced graphene oxide supercapacitor with large volumetric capacitance and ultralong stability prepared by electrophoretic deposition method, ACS Appl. Mater. Interfaces 7 (2015) 1348–1354, https://doi.org/10.1021/am507656q.
[27] Shalu, V.K. Singh, R.K. Singh, Development of ion conducting polymer gel electrolyte membranes based on polymer PVdF-HFP, BMIMTFSI ionic liquid and the Li-salt with improved electrical, thermal and structural properties, J. Mater. Chem. C 3 (2015) 7305–7318, https://doi.org/10.1039/c5tc00940e.
[28] S. Siyahjani, S. Oner, P.K. Singh, C. Varlikli, Highly efficient supercapacitor using single-walled carbon nanotube electrodes and ionic liquid incorporated solid gel electrolyte, High Perform. Polym. 30 (2018) 971–977, https://doi.org/10.1177/0954008318772333.
[29] M.P.S. Mousavi, B.E. Wilson, S. Kashefolgheta, E.L. Anderson, S. He, P. Bühlmann, A. Stein, Ionic liquids as electrolytes for electrochemical double-layer capacitors: structures that optimize specific energy, ACS Appl. Mater. Interfaces 8 (2016) 3396–3406, https://doi.org/10.1021/acsami.5b11353.
[30] S. Ozdemir, C. Varlikli, I. Oner, K. Ocakoglu, S. Icli, The synthesis of 1,8-naphthalimide groups containing imidazolium salts/ionic liquids using I-, PF6-, TFSI- anions and their photophysical, electrochemical and thermal properties, Dyes Pigments 86 (2010) 206–216, https://doi.org/10.1016/j.dyepig.2010.01.005.
[31] B. Pal, S. Yang, S. Ramesh, V. Thangadurai, R. Jose, Electrolyte selection for supercapacitive devices: a critical review, Nanoscale Adv. 1 (2019) 3807–3835, https://doi.org/10.1039/c9na00374f.
[32] Z.-B. Zhou, H. Matsumoto, K. Tatsumi, Low-melting, low-viscous, hydrophobic ionic liquids: aliphatic quaternary ammonium salts with perfluoroalkyltrifluoroborates, Chem. Eur J. 11 (2005) 752–766, https://doi.org/10.1002/chem.200400817.
[33] S. Sahoo, K. Krishnamoorthy, P. Pazhamalai, V.K. Mariappan, S. Manoharan, S. J. Kim, High performance self-charging supercapacitors using a porous PVDF-ionic liquid electrolyte sandwiched between two-dimensional graphene electrodes, J. Mater. Chem. 7 (2019) 21693–21703, https://doi.org/10.1039/c9ta06245a.
[34] Z. He, Q. Cao, B. Jing, X. Wang, Y. Deng, Gel electrolytes based on poly (vinylidenefluoride-co-hexafluoropropylene)/thermoplastic polyurethane/poly (methyl methacrylate) with in situ SiO2 for polymer lithium batteries, RSC Adv. 7 (2017) 3240–3248, https://doi.org/10.1039/c6ra25062a.
[35] A. Eftekhari, Supercapacitors utilising ionic liquids, Energy Storage Mater. 9 (2017) 47–69, https://doi.org/10.1016/j.ensm.2017.06.009.
[36] C.W. Liew, S. Ramesh, A.K. Arof, Good prospect of ionic liquid based-poly(vinyl alcohol) polymer electrolytes for supercapacitors with excellent electrical, electrochemical and thermal properties, Int. J. Hydrogen Energy 39 (2014) 2953–2963, https://doi.org/10.1016/j.ijhydene.2013.06.061.
[37] R. de Levie, On porous electrodes in electrolyte solutions. I. Capacitance effects, Electrochim. Acta 8 (1963) 751–780, https://doi.org/10.1016/0013-4686(63)80042-0.
[38] A. Izadi-Najafabadi, S. Yasuda, K. Kobashi, T. Yamada, D.N. Futaba, H. Hatori, M. Yumura, S. Iijima, K. Hata, Extracting the full potential of single-walled carbon nanotubes as durable supercapacitor electrodes operable at 4 V with high power and energy density, Adv. Mater. 22 (2010) E235–E241, https://doi.org/10.1002/adma.200904349.
[39] S. Zhang, N. Pan, Supercapacitors performance evaluation, Adv. Energy Mater. 5 (2015) 1–19, https://doi.org/10.1002/aenm.201401401.